

Role of spectral resolution for infrared asteroid compositional analysis using meteorite spectra

A. Skulteti,^{1*} A. Kereszturi,² Zs. Kereszty,³ B. Pal,^{2,5} M. Szabo,⁴ F. Cipriani⁶

¹Research Centre for Astronomy and Earth Sciences, Geographical Institute, MTA Centre of Excellence, Hungary

²Research Centre for Astronomy and Earth Sciences, Konkoly Thege Miklos Astronomical Institute, MTA Centre of Excellence, Hungary

³International Meteorite Collectors Association

⁴Research Centre for Astronomy and Earth Sciences, Institute for Geological and Geochemical Research, MTA Centre of Excellence, Hungary

⁵Eötvös Loránd University, Budapest, Hungary

⁶European Space Agency, ESTEC/TEC-EPS, Keplerlaan 1, 2200AG, Noordwijk

Accepted XXX. Received YYY; in original form ZZZ

ABSTRACT

In this work the potential mineral identification of meteorites is analysed for the mid-infrared range, to evaluate observational possibilities for future missions targeting small body surfaces. Three carbonaceous and three ordinary chondrite meteorites are examined by a diffuse reflection (DRIFT) instrument, and the presence of principal minerals is confirmed by a powder diffraction method as well. The possibilities and constraints of mineral identifications in the mid-infrared are simulated by artificially degrading the spectral resolution. Our research shows that for the definite identification of principal mineral bands, a spectral resolution $\leq 10 \text{ cm}^{-1}$ ($\leq 0.15 \mu\text{m}$) is needed. At $20\text{-}100 \text{ cm}^{-1}$ ($0.3\text{-}1.5 \mu\text{m}$) resolution the identification of these minerals is uncertain, and with a resolution $> 100 \text{ cm}^{-1}$, it is almost impossible.

Key words: minor planets, asteroids, meteorites

1 INTRODUCTION

The compositional analysis of asteroids is becoming more important, not only to reconstruct better the formation processes in the Solar System, but also to advance the understanding of possible methods and consequences of mitigating the threat of potentially hazardous Near Earth Asteroids (Trigo-Rodríguez et al. 2017), with meteorites providing direct information about them (Tásh et al. 2011), (Madiedo et al. 2013; Bland et al. 1996; Przylibski et al. 2003, 2005). More recently, the search for the parent bodies of possible meteorites (Trigo-Rodríguez et al. 2007; Gayon-Markt et al. 2012) has widened, partly focusing on spectral matching between asteroids and meteorites (Bowey et al. 2007; Trigo-Rodríguez et al. 2013), which could provide information on asteroid regoliths (Hamm et al. 2019a). Several missions were launched towards such asteroids in the last few years, including Hayabusa-1 (Yano et al. 2006) and Osiris-Rex (McMahon et al. 2018; Seabrook et al. 2019), Hayabusa-2 (Castelvecchi 2018; Michikami et al. 2019; Kitazato et al. 2019; Hamm et al. 2019b). Further afield, Dawn has targeted two large main belt asteroids (Park et al. 2016; Voosen 2018). Beyond the scientific aims, resource utilization is being considered for

future missions, because some components of Near Earth Asteroids might be exploitable (Luszczek & Przylibski 2019).

More missions have been proposed to target Near Earth asteroids recently with cubesats (Kohout et al. 2018) accompanying them, for example the DART (Raducan et al. 2019; Maindl & Schäfer 2019) and HERA missions (Michel et al. 2019; Tsiganis et al. 2019; Carnelli & Kueppers 2019; Kueppers et al. 2019). The use of cubesats is expected to increase in the next decades (Andrews et al. 2019; Cheng et al. 2019; Shkolnik 2018) along with the improved miniaturization of various electronics and detectors. Therefore, it is worth to consider and evaluate the mineral analysing capabilities of simple and cheap infrared detectors (Holland et al. 2018; Ardila et al. 2017), which will probably fly regularly on such small probes.

The results of this research could be applied to other Solar System bodies as well, for example Phobos and Deimos, the two moons of Mars, targeted by the MMX (Campagnola et al. 2018; D’Amore et al. 2019) mission planned by JAXA. The origin of these two satellites is still debated, whether they are captured asteroids (Burns 1978; Hartmann 1990) or formed in place (Craddock 2011). Their roughly circular orbits near the equatorial plane

* E-mail: skulteti.agnes@csfk.mta.hu

of Mars suggest *in-situ* formation, however, their visible and near-infrared spectra imply the capture theory. The spectra of Phobos and Deimos show similarities to D- or T-type asteroids or carbonaceous chondrites (Fraeman et al. 2014; Miyamoto et al. 2018), and their spectral characteristics are mostly similar to those of Tagish Lake and CM2 chondrites. Thus, our research could be useful in the design of future missions targeting these bodies.

This work aims to better understand the observational possibilities of the middle infrared spectra based mineral identification (Martin et al. 2019; MacLennan & Emery 2018), as this range provides more and detailed information on the composition than the more exploited near infrared range (Fulvio et al. 2018). Using meteorite samples (Gilmour et al. 2019), the almost intact interior of asteroids could be analysed (Donaldson Hanna et al. 2019). Nonetheless, in reality due to space weathering produced modifications (Fiege et al. 2019; Loeffler et al. 2018; Penttilä et al. 2014), even future close-by observations might not be able to identify minerals as evidently as presented here. The laboratory based references provide important experiences for the design of middle infrared detectors, especially their channel arrangements.

2 METHODS

In this work, the DRIFT measurements based infrared spectra of some meteorites were analysed and compared using a Vertex FTIR 70 infrared spectrometer plus a Harrick based DRIFT unit called Praying Mantis, used at room temperature. The spectral resolution is $0.04 \mu\text{m}$ (4 cm^{-1}), with 256 scans covering a wavelength range of $2.5\text{-}25 \mu\text{m}$ ($4000\text{-}400 \text{ cm}^{-1}$). Before the measurements WERE MADE, the meteorite powders were ground down to grain sizes $<50 \text{ \AA}$, with the majority of the grains in the $10\text{-}20 \text{ \AA}$ range. The materials were dried by baking them at $+120 \text{ \AA}$ for 12 hours in an oven prior to the measurements. The meteorites were ordinary chondrites from NWA 869 (L4-6 S3 W1), NWA 5838 (H6 W1), NWA 6059 (L6 S2 W2/3) and carbonaceous chondrites from Allende (CV3), NWA 10580 (CO3, S2/3, W3), NWA 11469 (CV3 type S2/3 W3).

A Fritsch Pulverisette-23 Mini-Ball Mill with zirconium-oxide mortar and three zirconium-oxide ball sets was used to pulverise the samples. The instrument has a 10 ml volume zirconium-oxide mortar, and works with an adjustable frequency between 15 and 50 Hz, together with adjustable pulverising duration.

The identified goethite was probably formed from previously existing FeNi alloy in the meteorites during weathering on the Earth. In an ideal case, only non-weathered ($W=0$) meteorites should be analysed, however such meteorites are difficult to obtain. The infrared analysis here is on non-ideal, but accessible meteorite samples, providing useful results for the identification of various non-weathered silicate components. Further studies should focus on unweathered samples to identify possible differences between them and those analysed in this work.

The reflectance spectra were interpreted based on the spectral database of Liese (1975). Spectral coarsening was done by artificially degrading the resolution with simple mathematical averaging (eq. 1, eq. 2):

$$x_d = \frac{\sum_{n=1}^d x}{d} \quad (1)$$

$$\lambda_d = \frac{\sum_{n=1}^d \lambda}{d} \quad (2)$$

where x_d represents the new data point with the desired resolution, x the original data point, d the resolution divisor (the degradation factor), λ_d the wavelength of the new data point and λ the wavelength of the original data point. After averaging, the new reduced resolution was determined by eq. 3:

$$\text{res}_d = \lambda_d^1 - \lambda_d^0 \quad (3)$$

where res_d is the new resolution, and λ_d^0 and λ_d^1 are the first and the second wavelengths in the new data respectively.

While the detection characteristics (e.g. sensitivity along the observable range) of the detectors are different, a simple approach was followed here: the sensitivity was taken to be constant all along the range. This is a good enough approximation to compare the different band arrangements, as the aim was to see the general trends and general characteristics.

Control measurements using powder diffraction method was also applied, to have an independent estimation on the mineral composition of the analysed samples. For XRD measurements, we used a Rigaku Miniflex600 Bragg-Brentano powder-diffractometer. We milled 40 mg of the samples mixed it with 1.5 ml ethanol and dried it on a steel section to produce the XRD sample. In the Miniflex600, the X-ray source is Cu, and we used an accelerating voltage of 40 keV and a beam current of 20 mA. It uses a scintillation detector NaD graphite monochromator with a measurement time of 35 minutes. This method was applied to gain the compositional ratio listed in Table 2.

3 RESULTS

First, the compositional analysis related general aspects are presented using the infrared band positions employed for mineral analysis, followed by results of the powder diffraction measurements. The degraded meteorite spectra are then presented, followed by a discussion of the evaluation of mineral observational possibilities.

3.1 Mineral identification

The identification of minerals was done by the DRIFT spectral analysis, using the band positions in Table 1. Control measurements by powder diffraction method were also made to identify the compositional ratio of minerals, shown in Table 2.

Although there is up to 10% FeNi alloy in ordinary

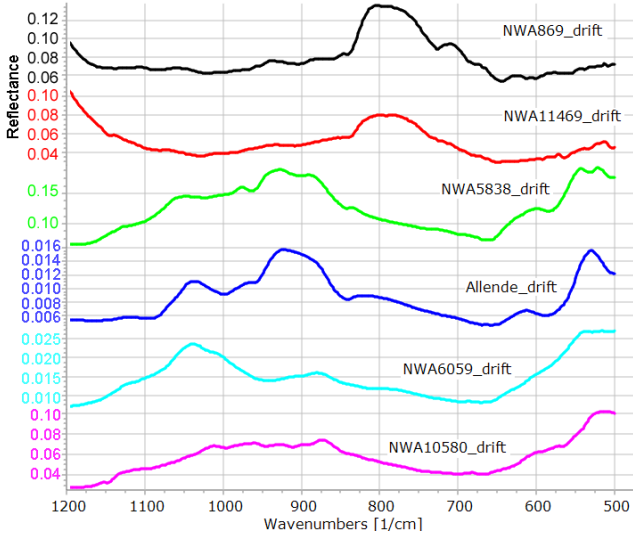


Figure 1. Mid-infrared reflectance curves of the analysed meteorites.

chondrites (Reisener & Goldstein 2003), the lack of its identification might be related to two factors: (1) the possible melting and partial destruction of FeNi alloy grains during pulverization, and (2) the fact that these minerals were partially weathered to various oxides and hydroxides, including goethite.

These meteorites contain several minerals with different grain sizes such that the superposition of individual peaks dominates the spectral shape, complicating interpretation.

The most important features of the reflectance spectra of silicates are the Christiansen and Restrahlen features. The wavelength of the Christiansen feature for individual minerals depends on polymerization (feldspar-shorter, mafic minerals: olivine, pyroxene longer wavelengths (Logan et al. 1973)). The Christiansen feature of pyroxene minerals is at a much shorter wavelength (8.5-8.4 Åµm) (~ 1180 cm $^{-1}$) than for olivine (Salisbury et al. 1991). The Christiansen feature of feldspar minerals is at a shorter wavelength (near 8 Åµm) (~ 1250 cm $^{-1}$) than for olivine and pyroxene. The Restrahlen bands of olivine are located at 9-11.5 Åµm (1100-870 cm $^{-1}$) (Mustard & Hays 1997), while its transparency band is located at approximately 12-15 Åµm (830-660 cm $^{-1}$).

3.2 Spectral coarsening

The observed spectra were artificially degraded to determine the minimum resolution required for the identification of key spectral features.

The main observable features are the common silicate mineral (olivine, pyroxene, and plagioclase) absorption bands related to iron ions. The fine details gradually disappear and the ability to identify the minerals gets worse with lower resolution. The disappearance of small peaks and fine details is clear, although the overall shape of the curves persists, even with poor spectral resolution. For example, the reflectance maxima around 800 or 1000 cm $^{-1}$ remains ob-

servable the longest, even at the lowest resolution in some cases.

4 DISCUSSION

The mineral observability is evaluated according to two different approaches: (A) The identification of more general spectral features, and (B) the identification of smaller specific mineral peaks. For the general appearance, the total shape of the curves and the following three general features were evaluated.

1. The Christiansen feature (CF, a reflectance minimum), due to a transition between the surface and volume scattering regime (Hapke 1996), appears as a reflectance minimum at ~ 1100 - 1300 cm $^{-1}$ (7.5-9 Åµm) in the case of silicates. In this wavelength region the refractive index changes rapidly, which causes minimal scattering. Thus, its exact peak positions could shift and possibly overlap with other features.

2. The Restrahlen bands (local maximum in reflectance) arise from fundamental molecular vibrations as most incident radiation does not enter the sample, but is reflected on the first surface. These peaks in the reflectance at ~ 1120 - 850 cm $^{-1}$ (8.5-12 Åµm) are by Si-O asymmetric stretching (however a less intense Restrahlen band appears around 750-300 cm $^{-1}$ (16.5-25 Åµm) by Si-O-Si bending).

3. The transparency feature (reflectance maximum) is located between two Restrahlen bands in the spectra of particulate silicates as a broad reflectance maximum, and is influenced by the presence of small particles (<75 Åµm) and changing optical constants. These features are diagnostic of the given minerals (e.g. Logan et al. (1973); Salisbury et al. (1991)).

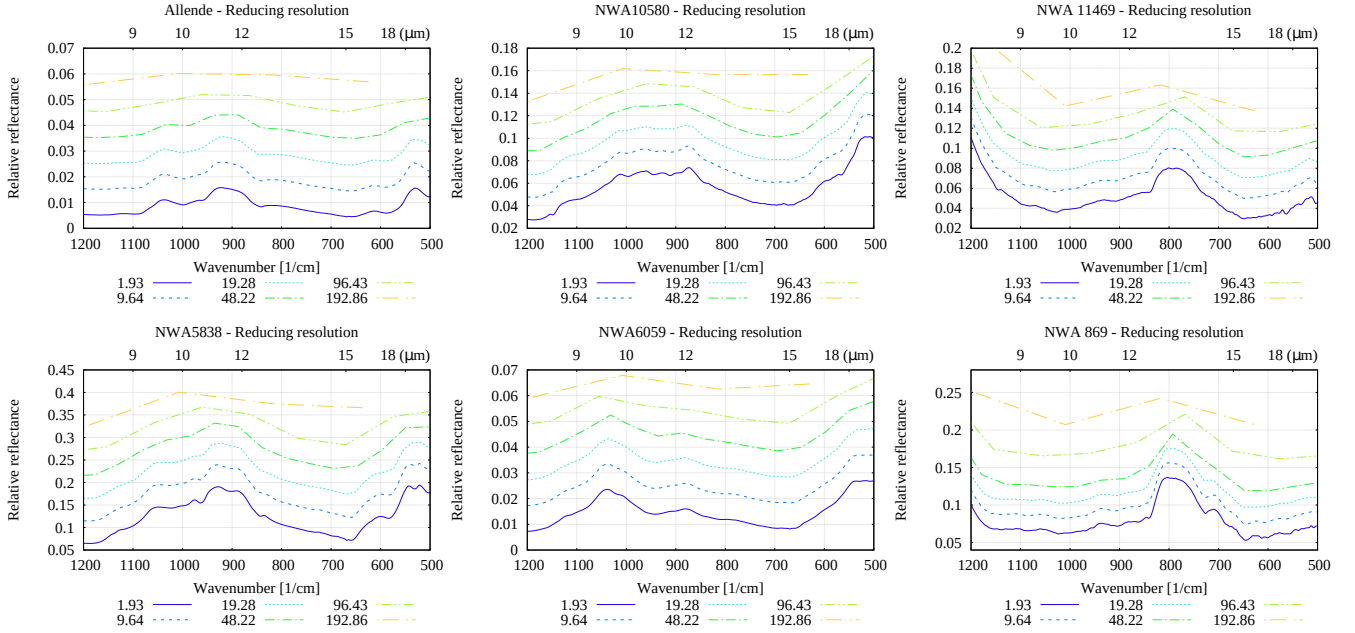
Comparing the observed spectral shapes, the evaluation of the Christiansen feature might be difficult due to its complex and changing appearance, and as it also could be influenced by the Restrahlen feature, which could overlap it. A reflectance minimum around the expected Christiansen feature was present in the case of Allende, NWA 5838, NWA 6059, NWA 10580, however it emerged, but shifted to longer wavelengths between 9-12 Åµm. This minimum seemed to be present in the spectrum of NWA 11469, but not with certainty. These observations suggest that if one aims to identify the band (and drop) in reflection compared to about 10-12 Åµm, it could be lost. If one searches for the edges of the band along different wavelengths but considers the range only at 8-9 Åµm, the Christiansen feature could be missed, as it might emerge at around 9-12 Åµm. It could also cause problems if there is a stronger reflection at the expected location, and no bands emerge relatively to the above mentioned Åµm location. The candidate bands for the Restrahlen feature appeared approximately at its expected location (8-12 Åµm) for NWA 869 AND NWA 11469. However, for the other four meteorites (Allende, NWA 5838, NWA 6059, NWA 10580) there was no band but just an occasionally elevated reflectance.

Table 1. Used infrared peak positions for mineral identification (*marks two different peaks which differ in shape also).

Meteorite	Peak positions used for mineral identification				
	olivine	pyroxene	feldspar	troilite	goethite
Allende	960, 842	669, 657	1092, 999	455	-
NWA 5838	960, 842	1023, 669, 675	999	-	904
NWA 10580	842	945, 911	1148, 1099, 999, 565	457	-
NWA 6059	842, 506	945, 669, 657	-	-	906
NWA 869	842	1028	727, 645	455	907
NWA 11469	837	1028	647, 565	457	908

Table 2. Mineral composition of meteorites used powder diffraction method.

Meteorite	Ratio of mineral components (%)				
	olivine	pyroxene	feldspar	troilite	goethite
Allende	47	35	116	2.155	0.3
NWA 5838	71.6	24	2.3	1.5	0.3
NWA 10580	62	21	12	4	1
NWA 6059	58	8.3	1.7	4	28
NWA 869	41.5	25	26.2	6.9	0.6
NWA 11469	26.8	21	28	0.3	23.9

**Figure 2.** Results of artificial spectral degradation of the 6 analysed meteorites. In each diagram highest resolution can be found at the bottom, and gradually lower resolution spectra by the indicated colours and line styles.

With low resolution, the Christiansen, Restrahlen and transparency features are not easily observable and thus are not ideal targets for identification. This is partly because they show variability; in fact, their detection is not straightforward even at high resolution. In the case of meteorites, The Christiansen feature is a combination of the characteristic CFs of all the constituent minerals. The Restrahlen features generally did not turn out to be a characteristic structure in the observed spectra, either. To summarize, to see the structure of Christiansen or Restrahlen bands, a spectral resolution of about 0.1 μm is required between 8-12 μm . In contrast, there were silicate rich meteorites that did not present these features, or at least not clearly. No general rule for the identification of silicate features could be found. This suggests that under non-ideal conditions, targeting $\tilde{\nu}$

$\tilde{\nu}$, space-weathered asteroid surfaces, the identification of these spectral features might be even more difficult. The variability between meteorites of the same type also suggests that any mineral identification method needs to be more general, requiring further testing.

4.1 Identification of specific minerals

It is probably more feasible to identify specific mineral identifiers than to rely on general spectral features. To evaluate this possibility at different spectral resolutions, the most important peaks of principal minerals (olivine, pyroxene, feldspar and goethite) were surveyed and characterized using the following grades: 2 $\tilde{\nu}$ evident band, 1 $\tilde{\nu}$ uncertain band, 0 $\tilde{\nu}$ no band visible (Table 3). To make firm

identifications of the main bands of mineral components, a spectral resolution better than 10 cm^{-1} ($0.15\text{ \AA}\mu\text{m}$) is required, with equally distributed bands in the $800\text{-}1000\text{ cm}^{-1}$ ($10\text{-}13\text{ \AA}\mu\text{m}$) range. The identification of these minerals is problematic and uncertain around resolution $20\text{-}100\text{ cm}^{-1}$ ($0.3\text{-}1.5\text{ \AA}\mu\text{m}$), and almost impossible with a resolution worse than $\sim 100\text{ cm}^{-1}$ ($1.5\text{ \AA}\mu\text{m}$).

Future research projects should cover lower weathering grade samples too, as here the otherwise present FeNi alloys were transformed to mainly goethite, but the results are still valid for silicates.

4.2 Proposed channel arrangement

Although the main bands of characteristic minerals could be identified, it is difficult to identify minerals successfully for all six meteorites using the same bands. In practice, any asteroid mission needs prepared for mineral identification using the same spectral set-up as lab-tested on related meteorites.

Two general problems emerge during the mineral identification. One is that bands of the same minerals might vary slightly, thus requiring a wider filter. However, this width is not large, as seen in Table 1. In the case of olivine, one key band ranged between $842\text{-}837\text{ cm}^{-1}$, while the other appeared in both cases at 960 cm^{-1} . For pyroxene, $657\text{-}669\text{ cm}^{-1}$ and $1023\text{-}1028\text{ cm}^{-1}$ were observed. In contrast, feldspar 999 and 565 did not change, while a shift between $1092\text{-}1099\text{ cm}^{-1}$ was observed for a third meteorite. For troilite the band was $455\text{-}457\text{ cm}^{-1}$, while for goethite it was $904\text{-}908\text{ cm}^{-1}$. In summary, where the same band appeared for different meteorites, the range of its shift was $\sim 4\text{-}9\text{ cm}^{-1}$, which might be wide enough for its identification.

The other difficulty was that for the same minerals different bands were observed for different meteorites e.g. a given band did not suffice for all meteorites. Table 3 gives the bands as a function of mineral and meteorite. Peaks are listed only if they were observed for at least two different meteorites. Despite all five minerals being present in each meteorite, they could be identified by the IR reflection spectra only in about half of the cases. As the analysed samples came from pulverized and homogenized powder of the meteorites, spatial compositional inhomogeneity could not produce this observed characteristic.

In agreement with the expectations, the concentration of minerals does not correlate with their dominance (and occasionally even their presence) in the spectra. Consequently, similar to laboratory results, the identification of given peaks does not correspond to concentration. However, a large or small areal occurrence at an asteroid surface might have a weak correlation with abundance (giving a rough upper limit for global occurrence). Based on theoretical considerations, crystalline structure (purity, homogeneity, and amorphous component ratio), grain size and possibly superposing spectral features from other minerals might cause the above identified diversity in the spectral identification of minerals.

Although the overall spectral shapes differed between the meteorites, NWA 869 (OC) and 11469 (CC) had some spectral similarities, as did NWA 5838 (OC) and Allende (CC). Considering their different types, there appears to be no characteristic trend. However, this may be expected as their main mineral components were the same. Additionally, the carbonaceous component probably does not have a major impact on the general spectral shape.

4.3 Instrumental experiences

Table 4 lists the basic spectral parameters for recently launched or planned asteroid missions. Most detectors would be able to identify the principal minerals in this study, although appropriate filters or selection of wavelengths would be necessary. Given the result that in roughly half of the cases a given mineral could be identified by multiple band features, assuming 3 filters for a given band identification, the identification of 3-4 minerals seems possible using 9-12 filters.

5 CONCLUSION

In this work the potential mineral identification of meteorites in the mid-infrared range as a function of spectral resolution was studied, in order to evaluate similar observational possibilities for asteroid surfaces by future space missions. Altogether 3 carbonaceous and 3 ordinary chondrite meteorites were investigated by a diffuse reflection providing DRIFT instrument. The existence of principal minerals was confirmed by a power diffraction method as a comparison to the infrared analysis.

Spectral bands covering $800\text{-}1000\text{ cm}^{-1}$ ($10\text{-}13\text{ \AA}\mu\text{m}$) were used to infer the mineral composition. Three potential issues were evaluated using the observed infrared reflectances. As expected, the dominance and strength of certain peaks of a given mineral do not correlate with its abundance/concentration in the sample. The same mineral might produce different peaks in different samples, making it hard to specifically identify its presence using a few predefined band positions. As a result, during the detector design phase, more peaks for one mineral should be considered. The most useful positions based on the laboratory survey of this work are the following: olivine: $842, 960\text{ cm}^{-1}$; pyroxene $657, 669, 945, 1023\text{ cm}^{-1}$; feldspar: $565, 999, 1092\text{ cm}^{-1}$; troilite: 455 cm^{-1} ; and goethite: 904 cm^{-1} .

The identification of principal minerals at different resolutions (by artificially degrading the spectra) was compared. For definite identification of the main mineral bands, resolution of $<10\text{ cm}^{-1}$ ($0.15\text{ \AA}\mu\text{m}$), with equally distributed bands. Around $20\text{-}100\text{ cm}^{-1}$ ($0.3\text{-}1.5\text{ \AA}\mu\text{m}$) resolution the identification is uncertain, and it is not possible with a resolution $>100\text{ cm}^{-1}$ ($1.5\text{ \AA}\mu\text{m}$).

Mission planners should be prepared to design mid-infrared spectrographs to cover multiple band features for a given mineral. Based on a sample of six carbonaceous and ordinary chondrite meteorites, the most important ones

Res./ Pos. (cm ⁻¹)	Allende					NWA 5838					NWA 10580					NWA 6059					NWA 869					NWA 11469							
	olivine	pyroxene	feldspar	olivine	pyroxene	feldspar	goethite	olivine	pyroxene	feldspar	olivine	pyroxene	feldspar	olivine	pyroxene	goethite	olivine	pyroxene	feldspar	goethite	olivine	pyroxene	feldspar	goethite									
	960	842	69-65	1092	999	960	842	1023	69-65	999	904	842	945	911	###	###	999	565	842	506	945	69-65	906	842	1028	727	645	907	837	1028	645	565	907
1.93	2	2	2	2	2	2	2	2	2	2	2	2	2	2	2	2	2	2	1	2	2	2	2	2	2	2	2	2	2	2	2	2	2
9.64	2	2	2	2	2	2	2	2	2	2	2	1	2	2	2	1	2	1	1	0	2	2	1	2	2	2	2	2	2	2	2	2	2
19.3	2	2	2	2	2	2	2	2	2	2	1	1	1	1	2	1	2	1	1	0	2	2	0	2	1	2	2	2	2	2	2	2	2
48.2	1	2	2	2	1	0	2	1	2	1	0	0	0	0	2	1	0	0	0	0	2	2	0	2	0	0	2	0	1	2	2	0	1
96.4	0*	0	2	0	0	0*	0	0	2	0	0	0	0	0	2	0	0	0	0	0	2	0	2	0	0	1	0	0	1	0	0*	0	
193	0	0	0	0	0	0	0	0	0	0	0	0	0	0	0	0	0	0	0	0	0	0	0	0	0	0	0	0	0*	0	0	0	0

Figure 3. Overview of the observability of selected spectral band positions, characteristic for the given minerals.

Table 3. Occurrence of specific mineral bands on the analysed meteorites in units of cm⁻¹. Only those bands are listed where they are observed in at least two meteorites.

Meteorite	Olivine		Pyroxene				Feldspar			Troilite	Goethite
	842	960	657	669	945	1023	565	999	1092	455	904
Allende	X	X	X	X			X	X	X		
NWA 869						X			X	X	
NWA 5838	X	X	X	X		X		X		X	
NWA 6059			X	X	X						X
NWA 10580	X				X	X	X	X	X		
NWA 11469						X	X			X	X

Table 4. Characteristics of mid-infrared detectors of recently launched and planned missions.

Mission name (target object)	Instrument name	Covered range	Spectral resolution	References and/or example results
BepiColombo (Mercury)	MERTIS (MERcury Radiometer and Thermal Infrared Spectrometer)	7-14 Åµm	0.09 Åµm	Hiesinger et al. (2018)
MarcoPolo-R (asteroid, cancelled)	THERMAP (THERMalMapper)	8-16 Åµm	0.3 Åµm	Groussin et al. (2016)
Osiris-Rex (Bennu)	OTES (Osiris-Rex Thermal Emission Spectrometer)	4-50 Åµm	0.15 Åµm	Christensen et al. (2018)
Hayabusa-2 (Ryugu)	Thermal Infrared Imager (TIR)	8-12 Åµm	0.02 Åµm	Okada et al. (2018)
Hayabusa-2 MASCOT lander (Ryugu)	MicrOmega	0.99-3.65 Åµm	0.3 Åµm	Bibring et al. (2017)
Lunar Reconnaissance Orbiter (Moon)	Diviner Lunar Radiometer Experiment	0.3-400 Åµm	9 channels	Chin et al. (2007)
AIM, HERA mission (Didymos asteroid)	TIRI	MIR	7-10 channels	Manzillo et al. (2018)

have been identified. These findings might have special importance in the case of cubesats, as this probe class is getting involved more frequently in space missions. On-board cubesats' low cost infrared detectors could provide optimised data, if the filter or band positions are carefully selected. Results of this work provide a basis for the refinement of future spectral band selection.

ACKNOWLEDGEMENTS

This work was supported by the NEOMETLAB project of ESA for the spectral data, by the Excellence of Strategic R&D centres (GINOP-2.3.2-15-2016-00003) project of NK-FIH and the related H2020 fund FOR the meteorite sample access, by the GINOP 2.3.2-15-2016-00009 for the mineral composition of meteorites, and by the the ÁZMKP-19-3 New National Excellence Program of the Ministry for Innovation and Technology.

REFERENCES

- Andrews D., Wahlund J.-E., Kohout T., Penttilä A., 2019, in EPSC-DPS Joint Meeting 2019. pp EPSC-DPS2019-1287
- Ardila D. R., Shkolnik E., Gorjian V., 2017, in American Astronomical Society Meeting Abstracts #229. p. 206.05
- Bibring J.-P., et al., 2017, [Space Science Reviews](#), 208, 401
- Bland P. A., Smith T. B., Jull A. J. T., Berry F. J., Bevan A. W. R., Cloudt S., Pillinger C. T., 1996, [Monthly Notices of the Royal Astronomical Society](#), 283, 551
- Bowey J. E., Morlok A., KÄuhler M., Grady M., 2007, [Monthly Notices of the Royal Astronomical Society](#), 376, 1367
- Burns J. A., 1978, [Vistas in Astronomy](#), 22, 193
- Campagnola S., Yam C. H., Tsuda Y., Ogawa N., Kawakatsu Y., 2018, [Acta Astronautica](#), 146, 409
- Carnelli I., Kueppers M., 2019, [Acta Astronautica](#), 156, 250
- Castelvecchi D., 2018, [Nature](#), 558, 495
- Cheng A., Rivkin A., Chabot N., Dotto E., 2019, in EPSC-DPS Joint Meeting 2019. pp EPSC-DPS2019-24
- Chin G., et al., 2007, [Space Science Reviews](#), 129, 391
- Christensen P. R., et al., 2018, [Space Sci. Rev.](#), 214, 87
- Craddock R. A., 2011, [Icarus](#), 211, 1150

- D'Amore M., et al., 2019, in Lunar and Planetary Science Conference. Lunar and Planetary Science Conference. p. 2383
- Donaldson Hanna K. L., et al., 2019, *Icarus*, **319**, 701
- Fiege K., Guglielmino M., Altobelli N., Trieloff M., Srama R., Orlando T. M., 2019, *Journal of Geophysical Research (Planets)*, **124**, 1084
- Fraeman A. A., Murchie S. L., Arvidson R. E., Clark R. N., Morris R. V., Rivkin A. S., Vilas F., 2014, *Icarus*, **229**, 196
- Fulvio D., Ieva S., Perna D., Kanuchova Z., Mazzotta Epifani E., Dotto E., 2018, *Planet. Space Sci.*, **164**, 37
- Gayon-Markt J., Delbo M., Morbidelli A., Marchi S., 2012, *Monthly Notices of the Royal Astronomical Society*, **424**, 508
- Gilmour C. M., Herd C. D. K., Beck P., 2019, *Meteoritics and Planetary Science*, **54**, 1951
- Groussin O., et al., 2016, *Experimental Astronomy*, **41**, 95
- Hamm M., Senshu H., Grott M., 2019a, *Icarus*, **319**, 308
- Hamm M., et al., 2019b, in EPSC-DPS Joint Meeting 2019. pp EPSC-DPS2019-1598
- Hapke B., 1996, *Journal of Geophysical Research: Planets*, **101**, 16833
- Hartmann W. K., 1990, *Icarus*, **87**, 236
- Hiesinger H., et al., 2018, in Lunar and Planetary Science Conference. Lunar and Planetary Science Conference. p. 1997
- Holland W., et al., 2018, in Proc. SPIE. p. 106981T, doi:10.1117/12.2311431
- Kitazato K., et al., 2019, *Science*, **364**, 272
- Kohout T., et al., 2018, *Advances in Space Research*, **62**, 2239
- Kueppers M., Michel P., Carnelli I., Ulamec S., Abell P. A., 2019, in Lunar and Planetary Science Conference. Lunar and Planetary Science Conference. p. 2567
- Liese C. H., 1975, in C. K., ed., *Infrared and Raman Spectroscopy of Lunar and Terrestrial Minerals*. Academic press, p. 390
- Loeffler M. J., Thompson M., Keller L. P., 2018, in AGU Fall Meeting Abstracts. pp P21D-3381
- Logan L. M., Hunt G. R., Salisbury J. W., Balsamo S. R., 1973, *Journal of Geophysical Research (1896-1977)*, **78**, 4983
- Luszczek K., Przylibski T. A., 2019, *Planetary and Space Science*, **168**, 40
- MacLennan E., Emery J., 2018, in AAS/Division for Planetary Sciences Meeting Abstracts #50. AAS/Division for Planetary Sciences Meeting Abstracts. p. 404.11D
- Madiedo J. M., Trigo-Rodríguez J. M., Castro-Tirado A. J., Ortiz J. L., Cabrera-Cañó J., 2013, *Monthly Notices of the Royal Astronomical Society*, **436**, 2818
- Maindl T. I., Schäfer C. M., 2019, in EPSC-DPS Joint Meeting 2019. pp EPSC-DPS2019-1516
- Manzillo F. F., Babic L., Esposito M., 2018, in Didymos Observer Workshop Prague. p. abstract 19
- Martin A., Emery J., Lindsay S., 2019, in EPSC-DPS Joint Meeting 2019. pp EPSC-DPS2019-766
- McMahon J. W., Scheeres D. J., Hesar S. G., Farnocchia D., Chesley S., Lauretta D., 2018, *Space Sci. Rev.*, **214**, 43
- Michel P., Küppers M., Carnelli I., Martino P., 2019, in EPSC-DPS Joint Meeting 2019. pp EPSC-DPS2019-259
- Michikami T., et al., 2019, *Icarus*, **331**, 179
- Miyamoto H., et al., 2018, in Lunar and Planetary Science Conference. Lunar and Planetary Science Conference. p. 1882
- Mustard J. F., Hays J. E., 1997, *Icarus*, **125**, 145
- Okada T., et al., 2018, in Lunar and Planetary Science Conference. Lunar and Planetary Science Conference. p. 1403
- Park R. S., et al., 2016, *Nature*, **537**, 515
- Penttilä A., Kohout T., Väisänen T., Muinonen K., Martikainen J., Markkanen J., Peltoniemi J., 2014, in AAS/Division for Planetary Sciences Meeting Abstracts #46. AAS/Division for Planetary Sciences Meeting Abstracts. p. 414.15
- Przylibski T. A., Pilski A. S., Zagożdżon P. P., Kryza R., 2003, *Meteoritics and Planetary Science*, **38**, 927
- Przylibski T. A., Zagożdżon Paweł P., Kryza R., Pilski A. S., 2005, *Meteoritics and Planetary Science Supplement*, **40**, 185
- Raducan S. D., Davison T. M., Luther R., Collins G. S., 2019, *Icarus*, **329**, 282
- Reisener R. J., Goldstein J. I., 2003, *Meteoritics & Planetary Science*, **38**, 1669
- Salisbury J. W., D'Aria D. M., Jarosewich E., 1991, *Icarus*, **92**, 280
- Seabrook J. A., et al., 2019, *Planet. Space Sci.*, **177**, 104688
- Shkolnik E. L., 2018, *Nature Astronomy*, **2**, 374
- Trigo-Rodríguez J. M., et al., 2007, *Monthly Notices of the Royal Astronomical Society*, **382**, 1933
- Trigo-Rodríguez J. M., et al., 2013, *Monthly Notices of the Royal Astronomical Society*, **437**, 227
- Trigo-Rodríguez J., Gritsevich M., Palme H., 2017, *Assessment and Mitigation of Asteroid Impact Hazards*. Vol. 46, doi:10.1007/978-3-319-46179-3,
- Tsiganis K., Kueppers M., Michel P., Carnelli I., Ulamec S., Cheng A., 2019, in EGU General Assembly Conference Abstracts. EGU General Assembly Conference Abstracts. p. 13147
- Tãșth J., Vereș P., Kornoș L., 2011, *Monthly Notices of the Royal Astronomical Society*, **415**, 1527
- Voosen P., 2018, *Science*, **362**, 275
- Yano H., et al., 2006, *Science*, **312**, 1350

This paper has been typeset from a $\text{\TeX}/\text{\LaTeX}$ file prepared by the author.